Determination of Internal Gas Flows by a Transient Numerical Technique

RAYMOND A. SERRA*
Pratt and Whitney Aircraft, East Hartford, Conn.

A time-dependent numerical method is developed for inviscid mixed subsonic-supersonic flows with shocks. The analysis is based on the Lax-Wendroff procedure but adds special treatments of the boundary conditions, a mapping of the physical contours and a damping term to provide stable solutions for planar and axisymmetric passages of arbitrary shape. Both transient and steady-state flows are computed with special emphasis being placed on the analysis of rapidly accelerating flows in axisymmetric ducts with sharp wall curvature. Results obtained compare favorably with experimental data and with prior analyses in those restricted regions where they have been applicable. In particular, excellent agreement is achieved between the present theory and experiment for the previously unsolved case of mixed flows in nozzles involving rapid subsonic contractions, sharp wall curvature at the throat and shocks in the supersonic flow portion. Here normal comparison parameters such as centerline and wall Mach number distributions, sonic line position and discharge coefficient are matched to a high degree of accuracy.

I. Introduction

In recent years a better understanding of the flow behavior and improved performance evaluations for rapidly expanding duct flows with shock waves have assumed considerable importance for many propulsion applications. This particularly applies to rapidly accelerating flows in nozzles characterized by a rapid contraction at the entrance, sharp wall curvature at the throat and near parallel flow at the exit.

For such nozzles the prediction of streamline distribution, discharge coefficient and downstream flow conditions, all of which determine the over-all thrust, is strongly affected by the representation of the possible shock pattern in the divergent section of the nozzle and by the nature of the analytical approximations that are made in the neighborhood of the throat and in the convergent nozzle section. Moreover, all of these flow conditions in turn affect the boundary-layer and heat transfer calculations which also have a significant influence on the performance prediction. Thus, there is a substantial need for accurate solutions of mixed flows throughout the entire passage of a nozzle.

In the past, progress in this area has been significantly hampered by the difference in the mathematical character of the governing equations for the subsonic and supersonic regions. As shown in Ref. 1, a survey of existing transonic nozzle solutions indicates that the majority of these studies entail either separate analyses in these regions which are matched across a transonic region by locally introducing a simplified flowfield or alternately involve an indirect approach where the channel contour is constructed from a specified velocity distribution along a suitable reference line.

In the former case, the resulting simplifications have led to solutions which provide inconsistent results near the matching sections and are limited to irrotational flows in nozzles with moderate wall curvature. On the other hand the sophisticated techniques required by the inverse procedure for iteratively matching centerline velocity distributions and computed streamlines with a prescribed boundary geometry are impractical for performance calculations and can produce unrealistic solutions in regions far removed from the throat. Moreover, the inverse procedure cannot be extended to rotational flows with shocks since the irrotationality condition is basic to the logic of the method.

The purpose of this paper is to overcome these limitations by presenting a transient numerical method of analysis for internal, inviscid, rotational flows with shocks over a wide Mach number range ($0 \leqq MN \leqq 5$) in either two-dimensional or axisymmetric finite nozzles. The validity of the method and the computed flowfields are substantiated by comparisons with experimental data.

II. Development of the Time Dependent Equations of Motion

A time dependent solution which treats the mixed flow problem as an initial value problem in time eliminates the need for treating the flow regimes independently and provides a direct approach for establishing the flowfield with a given boundary geometry and specified entrance conditions. This then permits either the solution of a true time dependent problem with emphasis on the transient nature of the flow or the relaxation of an initially assumed one-dimensional flow distribution to the two-dimensional or axisymmetric steady state solution.

The present numerical procedure for solving the unsteady equations of inviscid two-dimensional flow was originally formulated by Lax and Wendroff[2] and later extended to the axisymmetric case by Burstein.[3] This technique has been applied to the general nozzle problem by several authors, notably Moretti, et al.,[4] Prozan (as reported by Stephens[5] and Back, et al.[6]), and Wehofer and Moger.[7] However, in general, their results suffer from one or more serious shortcomings: the need for extensive smoothing in the calculation of the subsonic flowfield, the presence of numerical instabilities which arise from the formation of incipient shocks in the supersonic flow region, and the mathematical overspecification of the entrance flow conditions. This has led either to poor accuracy in the flowfield which resulted in the prediction of inaccurate nozzle discharge coefficients or to complex numerical procedures which require a substantial amount of computation time.

In order to eliminate these limitations, it is necessary to stabilize the numerical procedure in the vicinity of shocks and to establish realistic flow conditions at the entrance. In the present method this is achieved by including a numerical damping term based on the work of Burstein[3] and introducing a modified boundary calculation at the entrance.

Received December 18, 1970. Presented as Paper 71-45 at the AIAA 9th Aerospace Sciences Meeting, New York, January 25–27, 1971; revision received September 20, 1971. This paper is based on a thesis submitted in partial fulfillment of the requirements for the Ph.D. degree in the Graduate School of Mechanical Engineering, Rensselaer Polytechnic Institute. The author is grateful for the comments and suggestions of F. Landis of New York University.

Index categories: Nozzle and Channel Flow; Subsonic and Transonic Flow.

* Research Scientist. Member AIAA.

The assumptions concerning the transient model are essentially those made by Burstein[8]: The flow is inviscid and adiabatic, obeys the perfect gas law, has a constant molecular weight, but may have specific heats which vary with temperature. For two-dimensional ($\varepsilon = 0$) and axisymmetric ($\varepsilon = 1$) unsteady flow the governing equations per unit volume are written in divergence free form as the following vector equation:

$$\bar{W}_t = -\bar{F}_x - \bar{G}_y - (\varepsilon/y)\bar{H} \tag{1}$$

where

$$\bar{W} = \begin{bmatrix} \rho \\ L \\ M \\ E \end{bmatrix}, \quad \bar{F} = \begin{bmatrix} L \\ \dfrac{L^2}{\rho} + \tilde{g}P \\ L\dfrac{M}{\rho} \\ \dfrac{E+P/\tilde{J}}{\rho}L \end{bmatrix},$$

$$\bar{G} = \begin{bmatrix} M \\ \dfrac{L}{\rho}M \\ \dfrac{M^2}{\rho} + \tilde{g}P \\ \dfrac{E+P/\tilde{J}}{\rho}M \end{bmatrix}, \quad \bar{H} = \begin{bmatrix} M \\ \dfrac{L}{\rho}M \\ \dfrac{M^2}{\rho} \\ \dfrac{E+P/\tilde{J}}{\rho}M \end{bmatrix}$$

Here, ρ is the density, L and M are the x and y components of momentum, respectively, E is the total energy $[E = \rho(e + |\bar{q}|^2/2\tilde{g}\tilde{J})]$ and $\tilde{g}$ and $\tilde{J}$ are the gravitational and Joule's constants, respectively. Pressure P is expressed in terms of the other dependent variables by means of the equation of state $[P = P(\rho, e)]$.

The procedure for solving the equation system is based on a second-order Taylor series expansion of the dependent variable $\bar{W}$ in time

$$\bar{W}(x, y, t+\Delta t) = \bar{W}(x, y, t) + \bar{W}_t \Delta t + \bar{W}_{tt}\Delta t^2/2 \tag{2}$$

and follows the methods of Refs. 2 and 8 except that the specific heat ratio is allowed to vary with temperature. The evaluation of the differentials $d\bar{F}$, $d\bar{G}$ and $d\bar{H}$ in terms of the above dependent variables enables $\bar{W}_{tt}$ to be expressed as

$$\bar{W}_{tt} = [\hat{A}(\bar{F}_x + \bar{G}_y + (\varepsilon/y)\bar{H})]_x + [\hat{B}(\bar{F}_x + \bar{G}_y + (\varepsilon/y)\bar{H})]_y + (\varepsilon/y)[\hat{C}(\bar{F}_x + \bar{G}_y + \bar{H}/y)] \tag{3}$$

which, when combined with Eq. (1), establishes the basic equation system to be solved as

$$\bar{W}(x, y, t+\Delta t) = \bar{W}(x, y, t) - (\bar{F}_x + \bar{G}_y + (\varepsilon/y)\bar{H})\Delta t + \{[\hat{A}(\bar{F}_x + \bar{G}_y + (\varepsilon/y)\bar{H})]_x + [\hat{B}(\bar{F}_x + \bar{G}_y + (\varepsilon/y)\bar{H})]_y + (\varepsilon/y)[\hat{C}(\bar{F}_x + \bar{G}_y + \bar{H}/y)]\}\Delta t^2/2 \tag{4}$$

Here, the superscripts $\bar{}$ and $\hat{}$ refer to vector and matrix quantities, respectively, and matrices $\hat{A}$, $\hat{B}$ and $\hat{C}$, listed in Appendix A, represent the Jacobians of $\bar{F}$, $\bar{G}$ and $\bar{H}$ with respect to $\bar{W}$. A detailed derivation of the equation system and of the matrix evaluation can be found in Ref. 1. The system is accurate through second-order terms in Δt and is sufficient for the evaluation of a continuously accelerating flowfield.

III. Transformation to a Rectangular Domain

The system is applied to passage areas bounded by $x = 0$ and $x = x_{max}$ and contained between the curves $y = Y_L(x)$ and $y = Y_U(x)$ as shown in Fig. 1a. Note that for axisymmetric flow $Y_L(x) \geqq 0$. Unfortunately, the application of finite difference approximations to such a domain results in an unequally spaced grid in the neighborhood of the solid contours which complicates the formulation and frequently leads to numerical instabilities.

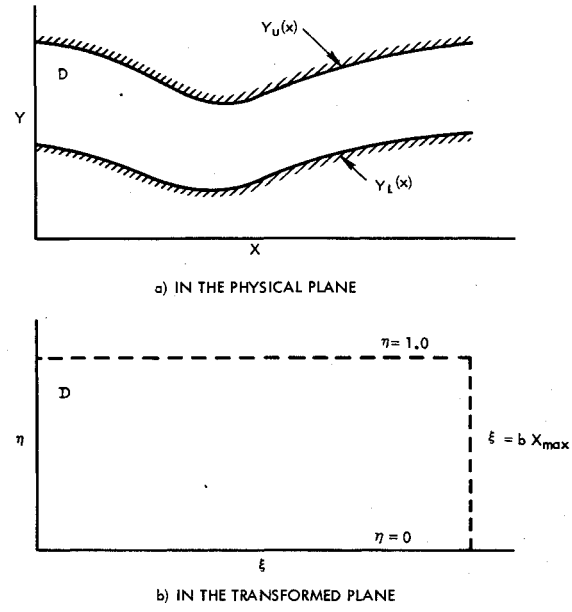

Fig. 1 Passage area.

These difficulties can be avoided by mapping an arbitrary passage into a rectangle from which an equally spaced mesh can be obtained via the following transformation of the independent spatial coordinates

$$\xi = bx \tag{5a}$$

and

$$\eta = [y - Y_L(x)]/[Y_U(x) - Y_L(x)] \tag{5b}$$

The domain D in the physical x-y plane is now mapped into the rectangular domain D in the ξ-η plane with sides ranging between $0 \leqq \xi \leqq bx_{max}$ and $0 \leqq \eta \leqq 1$ as shown in Fig. 1b.

Use of the chain rule enables the partial derivatives in the physical plane to be expressed as $(\,)_x = b(\,)_\xi + \alpha(\,)_\eta$ and $(\,)_y = \beta(\,)_\eta$ where

$$\beta = 1/[Y_U(x) - Y_L(x)], \qquad \alpha = -\beta\{\eta[(Y_U)_x - (Y_L)_x] + (Y_L)_x\}$$

and the scaling factor b is selected so that angles are approximately preserved under the transformation. The transformed system now becomes

$$\bar{W}(x, y, t+\Delta t) = \bar{W}(x, y, t) - \left[b\bar{F}_\xi + \alpha\bar{F}_\eta + \beta\bar{G}_\eta + \frac{\varepsilon}{y}\bar{H}\right]\Delta t + \left\{b\left[\hat{A}\left(b\bar{F}_\xi + \alpha\bar{F}_\eta + \beta\bar{G}_\eta + \frac{\varepsilon}{y}\bar{H}\right)\right]_\xi + \alpha\left[\hat{A}\left(b\bar{F}_\xi + \alpha\bar{F}_\eta + \beta\bar{G}_\eta + \frac{\varepsilon}{y}\bar{H}\right)\right]_\eta + \beta\left[\hat{B}\left(b\bar{F}_\xi + \alpha\bar{F}_\eta + \beta\bar{G}_\eta + \frac{\varepsilon}{y}\bar{H}\right)\right]_\eta + \frac{\varepsilon}{y}\left[\hat{C}\left(b\bar{F}_\xi + \alpha\bar{F}_\eta + \beta\bar{G}_\eta + \frac{H}{y}\right)\right]\right\}\frac{\Delta t^2}{2} \tag{6}$$

IV. Equations in Finite-Difference Form

Let $f_{i,j}$ designate the scalar value $f(i\Delta\xi, j\Delta\eta)$ for those values of i and j within the domain D. Vectors are represented at a point $(i\Delta\xi, j\Delta\eta)$ by a dual subscript and single superscript notation, $F_{i,j}^{\tau} = F_\tau(i\Delta\xi, j\Delta\eta)$, where the free superscript τ designates the components of the vector. Similarly, the components of a matrix at a point $(i\Delta\xi, j\Delta\eta)$ are denoted by the dual subscripts and superscripts, $A_{i,j}^{\tau,\mu} = A_{\tau,\mu}(i\Delta\xi, j\Delta\eta)$ where τ and μ denote rows and columns, respectively. The corresponding grid network for an interior point construction is shown on Fig. 2.

Setting $\Delta\xi = \Delta\eta = \Delta$, the finite difference expressions for $(\hat{A}\bar{F}_\xi)_\xi$, $(\hat{B}\bar{G}_\eta)_\eta$ and $(\hat{B}\bar{F}_\xi)_\eta$ using central differences can be written for an interior point $(i\Delta\xi, j\Delta\eta)$ as

$$[\hat{A}\bar{F}_\xi]_\xi = \sum_{\mu=1}^{4} \frac{1}{\Delta}\left[\frac{A_{i+1,j}^{\tau,\mu}+A_{i,j}^{\tau,\mu}}{2}\frac{F_{i+1,j}^{\mu}-F_{i,j}^{\mu}}{\Delta} - \frac{A_{i,j}^{\tau,\mu}+A_{i-1,j}^{\tau,\mu}}{2}\frac{F_{i,j}^{\mu}-F_{i-1,j}^{\mu}}{\Delta}\right] \tag{7a}$$

$$[\hat{B}\bar{G}_\eta]_\eta = \sum_{\mu=1}^{4} \frac{1}{\Delta}\left[\frac{B_{i,j+1}^{\tau,\mu}+B_{i,j}^{\tau,\mu}}{2}\frac{G_{i,j+1}^{\mu}-G_{i,j}^{\mu}}{\Delta} - \frac{B_{i,j}^{\tau,\mu}+B_{i,j-1}^{\tau,\mu}}{2}\frac{G_{i,j}^{\mu}-G_{i,j-1}^{\mu}}{\Delta}\right] \tag{7b}$$

and

$$[\hat{B}\bar{F}_\xi]_\eta = \sum_{\mu=1}^{4} \frac{1}{\Delta}\left\{\frac{B_{i,j+1}^{\tau,\mu}+B_{i,j}^{\tau,\mu}}{2}\times \frac{1}{2}\left[\frac{F_{i+1,j+1}^{\mu}-F_{i-1,j+1}^{\mu}}{2\Delta}+\frac{F_{i+1,j}^{\mu}-F_{i-1,j}^{\mu}}{2\Delta}\right] - \frac{B_{i,j}^{\tau,\mu}+B_{i,j-1}^{\tau,\mu}}{2}\times \frac{1}{2}\left[\frac{F_{i+1,j}^{\mu}-F_{i-1,j}^{\mu}}{2\Delta}+\frac{F_{i+1,j-1}^{\mu}-F_{i-1,j-1}^{\mu}}{2\Delta}\right]\right\} \tag{7c}$$

The resulting expression for $\bar{W}$ at time $t+\Delta t$ is obtained similarly by expression Eq. (6) in finite difference form as given by Eq. (B1) in Appendix B. A modified version of this equation is required for the axisymmetric calculation along the centerline as shown in Ref. 1.

The same difference equation is used at mesh points on solid contours bounding the flow. The use of an internal flow construction along the solid walls is achieved by using the reflection principle to establish flow properties at external virtual grid line points where the virtual grid line is a mirror image of the internal grid line immediately adjacent and parallel to the contour. In reality the principle is an approximate numerical technique which requires that the momentum normal to a solid wall be zero, the momentum tangent to a solid wall have a zero gradient across the wall, and the density and energy gradients across a solid wall be zero.

For a wall parallel to the x axis the reflection rule is simply $\rho_{i,j\pm1} = \rho_{i,j\mp1}$, $L_{i,j\pm1} = L_{i,j\mp1}$, $M_{i,j\pm1} = -M_{i,j\mp1}$ and $E_{i,j\pm1} = E_{i,j\mp1}$. The same rule applies for walls parallel to the y axis except that $L_{i\pm1,j} = -L_{i\mp1,j}$ and $M_{i\pm1,j} = M_{i\mp1,j}$. For a curved contour a more complicated construction is required which includes the determination of normals to the solid boundary, quadratic interpolation and the evaluation of derivatives in the transformed plane. Details are given in Ref. 1.

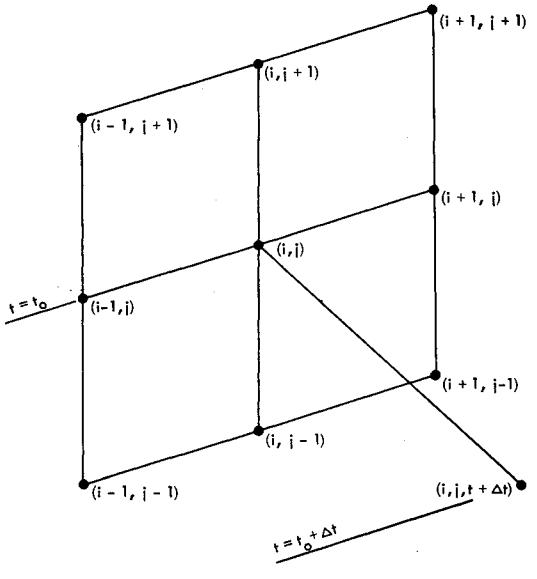

Fig. 2 Grid network for an interior point.

The linear stability limit established for Eq. 4 by Lax and Wendroff[2] can be expressed in the transformed plane as

$$\Delta t \leqq \Delta/[8^{1/2}b(u+a)], \qquad \Delta t \leqq \Delta/[8^{1/2}\beta(v+a)]$$

and is used as the basic stability criterion for all numerical calculations described herein. Here, u and v are the x and y components of velocity respectively, and a is the speed of sound. Recently, Burstein[3] has shown that numerical instabilities occur in the present finite difference procedure when constructing strong shocks in the vicinity of an axis of symmetry, transonic flowfields in passages with gentle wall curvature, and stagnation flows in the neighborhood of a blunt leading edge unless the following damping term is introduced.

$$\frac{\Delta t}{2}\left[\Delta^x(\hat{D}^x\Delta^x\bar{W}) + \Delta^y(\hat{D}^y\Delta^y\bar{W})\right]$$

Here Δ^x and Δ^y represent centered differences in the x and y directions, respectively, where as $\hat{D}^x$ and $\hat{D}^y$ are the corresponding dissipative matrices which are formulated in terms of $\hat{A}$ and $\hat{B}$ and their respective eigenvalues.

V. Formulation of the Transient Problem

A primary objective of the paper is to construct subsonic as well as subsonic-supersonic flow in a convergent-divergent finite nozzle. The unique solution sought must satisfy the steady-state equations of inviscid flow with the following prescribed boundary conditions: 1) the nozzle contour, 2) three independent flow conditions across the upstream subsonic entrance section, and 3) either a single downstream flow condition if the flow remains fully subsonic or, for supersonic exit flow, that the established solution smoothly joins the subsonic (elliptic) and supersonic (hyperbolic) portions of the flow. This formulation is totally consistent with that required by a well-posed problem whose solution is unique and continuous at the boundaries. In practice, condition 3 implies that once three independent upstream conditions are given, the specification of one downstream condition, such as the pressure, uniquely defines a fully subsonic flow where as in subsonic-supersonic flow the "choking condition" provides the sole requirement for the unique determination of the flow.

This solution is obtained by solving a transient, quasilinear, initial value problem which satisfies the identical boundary conditions and asymptotically reduces in time to the above steady state problem. An asymptotic solution is constructed which is continuous at the entrance and which satisfies the unsteady equations of motion for the prescribed boundary conditions listed above and for some initial flow distribution. This is unlike the approach utilized in Ref. 9 which requires the a priori specification of all upstream flow conditions and the subsequent admittance of weak (discontinuous) solutions at the entrance.

If this transient problem is linearized, its well posedness can be explicitly displayed through a uniqueness proof which employs the general theory of Symmetric Positive Linear Equations by Friedrichs.[10] The extension to the present quasilinear equation system is achieved by means of a standard iteration technique described in Ref. 11. In carrying out the actual details,[12] it can be established through the stability and consistency of the associated difference schemes that the time-independent solution to the transient problem is indeed the solution to the original steady-state problem.

In addition, it can be shown that the entrance and exit boundary data must follow certain constraints. In particular, it is found that the fourth entrance condition must be determined from a relationship which is precisely the interior characteristic compatibility condition. The compatibility relations for the present equation system are obtained conveniently by rewriting Eq. (1) as

$$\bar{W}_t + \hat{A}\bar{W}_x = -\hat{B}\bar{W}_y - (\varepsilon v/y)\bar{V} \tag{8}$$

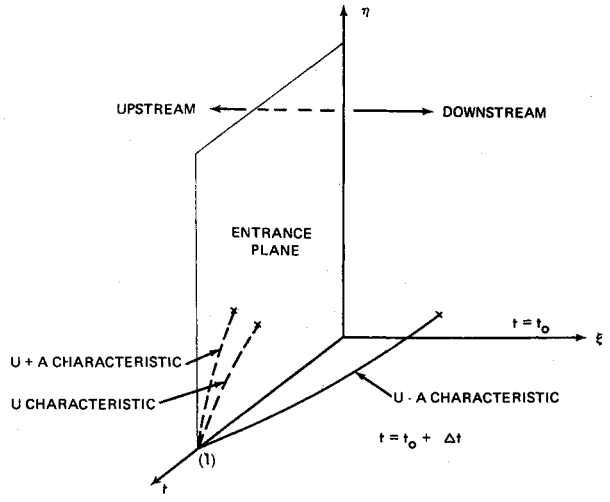

Fig. 3 Mach line construction at the entrance to a duct.

where

$$\bar{W}=\begin{bmatrix}\rho\\ u\\ v\\ P\end{bmatrix} \qquad \bar{V}=\begin{bmatrix}1\\ 0\\ 0\\ \dfrac{a^2}{\tilde{g}}\end{bmatrix}$$

$$\hat{A}=\begin{bmatrix}u & \rho & 0 & 0\\ 0 & u & 0 & \dfrac{\tilde{g}}{\rho}\\ 0 & 0 & u & 0\\ 0 & \dfrac{\rho a^2}{\tilde{g}} & 0 & u\end{bmatrix} \qquad \hat{B}=\begin{bmatrix}v & 0 & \rho & 0\\ 0 & v & 0 & 0\\ 0 & 0 & v & \dfrac{\tilde{g}}{\rho}\\ 0 & 0 & \dfrac{\rho a^2}{\tilde{g}} & v\end{bmatrix}$$

This equation is then written in normal form by first obtaining the eigenvalues (λ_g) and eigenvectors ($\bar{\zeta}^g$), $g = 1,\ldots,4$ of the matrix $\hat{A}$ from

$$\bar{\zeta}^g[\hat{A}-\lambda_g\hat{I}]=0 \tag{9}$$

where $\hat{I}$ is the identity matrix.

Noting that Eq. (9) possesses a nontrivial solution if and only if $|\hat{A}-\lambda_g\hat{I}|=0$ enables the eigenvalues of $\hat{A}$ to be determined as $\lambda_1=u$, $\lambda_2=u+a$, $\lambda_3=u-a$ and $\lambda_4=u$. The corresponding eigenvectors are obtained by equating the vector components of Eq. (9) to zero and requiring that the eigenvectors be linearly independent. This leads to the following expressions for $\bar{\zeta}^g$:

$$\bar{\zeta}^1=\left[-\frac{a^2}{\tilde{g}},\,0,\,1,\,1\right] \quad \bar{\zeta}^2=\left[0,\,\frac{\rho a}{\tilde{g}},\,0,\,1\right]$$

$$\bar{\zeta}^3=\left[0,\,-\frac{\rho a}{\tilde{g}},\,0,\,1\right] \quad \bar{\zeta}^4=\left[-\frac{a^2}{\tilde{g}},\,0,\,-1,\,1\right]$$

Equation (8) is now transformed into normal form by introducing the new vector, $\bar{Z}=\hat{U}\bar{W}$, premultiplying the resulting equation by $\hat{U}$, and applying the similarity transformation

$$\hat{T}=\hat{U}\hat{A}\hat{U}^{-1} \tag{11}$$

Here, $\hat{U}$ is the matrix whose rows are the eigenvectors, $\hat{U}^{-1}$ is the inverse of $\hat{U}$ and $\hat{T}$ is the diagonal matrix with the eigenvalues λ_g as its diagonal elements. The above sequence of operations permits the desired normal form of the equation system to be expressed as

$$\bar{Z}_t+\hat{T}\bar{Z}_x=-\hat{Y}\bar{Z}-\hat{X}\bar{Z}_y-(\varepsilon v/y)\hat{U}\bar{V} \tag{12}$$

where

$$\hat{Y}=\hat{U}[\hat{U}_t^{-1}+\hat{A}\hat{U}^{-1}+\hat{B}\hat{U}_y^{-1}]$$

and

$$\hat{X}=\hat{U}\hat{B}\hat{U}^{-1}$$

As illustrated in Fig. 3, the characteristic directions defined by

$$d_g(\,)\equiv(\,)_t+\lambda_g(\,)_x+v(\,)_y \tag{13}$$

show that the domain affecting an entrance point (1) at $t=t_0+\Delta t$ originates from a region which lies both upstream and downstream of the entrance at $t=t_0$. Therefore, the constraint is established from the compatibility relationship along the $u-a$ characteristic which emanates from the downstream region. This is obtained by writing Eq. (12) in component form and may be expressed as[1]

$$d_3(P)-(\rho a/\tilde{g})d_3(u)=(\rho a^2/\tilde{g})v_y-\varepsilon(\rho v/y)a^2/\tilde{g} \tag{14}$$

Hence, the formulation of entrance, timelike, boundary conditions is obtained by a priori specifying three independent flow conditions and calculating the remaining flow parameter via Eq. (14).

Similar arguments can be used to show that the formulation of the downstream timelike boundary conditions must be specified differently for subsonic and supersonic exit flows. In fully subsonic flows one flow condition is specified at the exit and the remaining flow parameters are obtained from the upstream compatibility relationships along the u and $u+a$ characteristics. The resulting time-dependent asymptotic solutions adjust to satisfy the three inlet and one exit boundary conditions.

In subsonic-supersonic flows, no arbitrary flow conditions are permitted to be prescribed at the nozzle exit. Here, an approximate initial flow distribution is assumed throughout the passage and exit boundary conditions are obtained by a linear extrapolation of the dependent variables at adjacent interior mesh points along an η grid line. This simple procedure is permissible only for a supersonic regime where the hyperbolic character of the equation system prevents errors introduced by the extrapolation from traveling upstream and affecting the interior flow calculation.

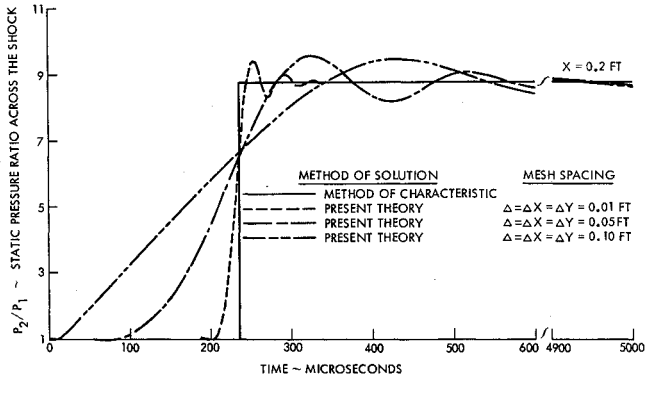

Fig. 4 Effect of mesh size on the finite-difference solution to the hammer shock problem.

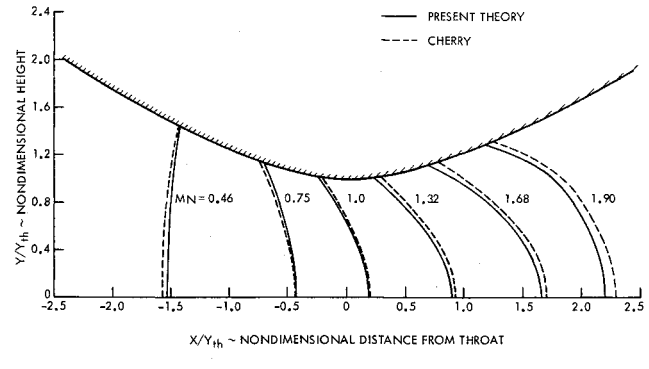

Fig. 5 Lines of constant Mach number in a two-dimensional modified hyperbolic nozzle.

To summarize, the boundary conditions which properly pose the transient initial value problem are: 1) the nozzle contour, 2) three independent upstream flow conditions for subsonic entrance flow, and 3) one (no) independent downstream flow condition(s) for subsonic (supersonic) exit flow. In addition, an initial flow distribution must be specified throughout the flowfield.

It is exactly this formulation which forms the basis for establishing the steady-state solutions displayed in Figs. 5–12. Specifically, the boundary conditions used are: the nozzle contours illustrated in the figures, entrance total pressure (P_0) and temperature (T_0) plus an assumed linear variation for the entrance flow angle, and the exit static pressure (P_e) for the fully subsonic flow cases (see Figs. 7 and 12). All initial flow distributions are determined by means of a one-dimensional flow approximation.

The values of P_0, T_0 and P_e are selected from available experimental data; a linear flow angle variation is imposed in the absence of any additional information. This selection of upstream flow variables has been based solely on the availability of the data and, as evidenced by the results, appears to be a realistic representation of the actual entrance flow conditions for the specific problems considered in the next section.

VI. Discussion of Results

Calculations using the present numerical technique were performed on an 1108 Univac digital computer for inviscid flows of mixed type in both two-dimensional and axisymmetric ducts. Steady state solutions were obtained by employing a variable grid spacing with spatial step size being varied during a calculation from a coarse ($\Delta = 0.1$) to a relatively fine ($\Delta = 0.01$) mesh. The criteria utilized for establishing steady state conditions are to match mass flow rates at prescribed axial locations to within 0.1% and to require during consecutive time steps that relative differences of selected flow parameters be less than 0.001%.

One-Dimensional Results

The program was initially checked out with various simple one-dimensional time-dependent problems, as typified by a hammer shock problem. Here a steady supersonic airstream ($MN = 2$) in a constant area duct of semi-infinite length is discharged into the atmosphere. At some prescribed time the closing of the duct exit produces a hammer shock which propogates upstream and stagnates the oncoming flow. According to the characteristic solution of Ref. 13, the shock passes a point 0.2 ft upstream of the exit after 235 μsec and causes the static pressure ratio to increase by a factor of 8.73.

Figure 4 displays the typically good agreement between the pressure-time distributions at a fixed location when the present technique is compared to the method of characteristics. The resolution time to approach the steady state rise with oscillations not in excess of 1% of this value correspond to less than 100 μsec for the fine mesh ($\Delta = 0.01$) as compared to approximately

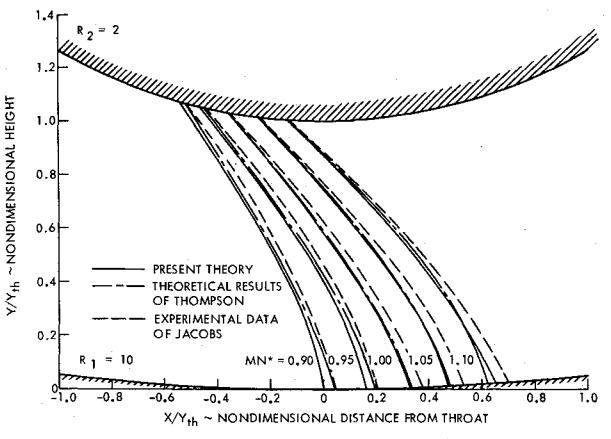

Fig. 6 Isovels in a two-dimensional curved channel.

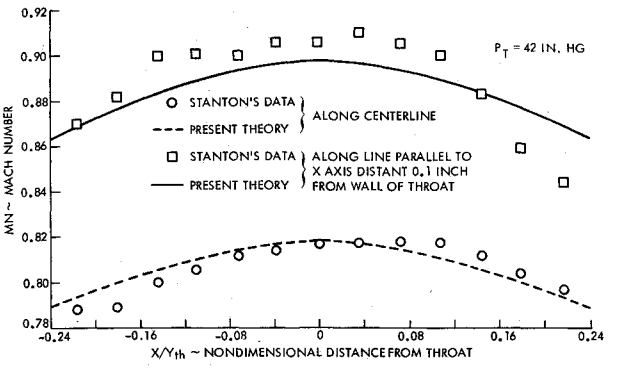

Fig. 7 Subsonic Mach number distribution in a circular-arc nozzle with $R = 4.77$.

5000 μsec for the coarse mesh ($\Delta = 0.1$). Hence, an order of magnitude reduction in mesh size shortens the resolution time by almost two orders of magnitude.

The possibility of achieving this fine resolution, though at the expense of increased computer time, is of prime importance for solving multiple and interacting transient shock problems. For this problem, over-all computing times ran from two minutes for the coarse mesh (121 points) to five and a half minutes for the fine mesh (611 points).

Two-Dimensional Results

A classical two-dimensional mixed flow problem is the sonic region of a convergent-divergent nozzle. Here the details of the sonic line depend on both the slopes and curvatures of the nozzle contour, especially in the vicinity of the throat. Figure 5 compares the present computational results with the analytical predictions of Cherry.[14] Both solutions produce Mach number profiles which are similar in shape but are slightly displaced from each other with the direction of displacement changing in the vicinity of the sonic line. This small shift may be attributed to the different flow conditions formulated at the nozzle inlet.

The effect of throat curvature on the velocity profile distribution is shown in Fig. 6 for a two-dimensional circular-arc channel. The results are compared to the modified series solution of Thompson[15] and the experimental data of Jacobs.[16] Agreement between experimental and computational results is within the limits of experimental resolution except near the large radius wall where the boundary layer has an important effect on experimental results.

Axisymmetric Results

Checkout calculations for axisymmetric nozzles permitted comparison with the experimental results of Stanton[17] for both fully subsonic and subsonic-supersonic flows in a circular-arc

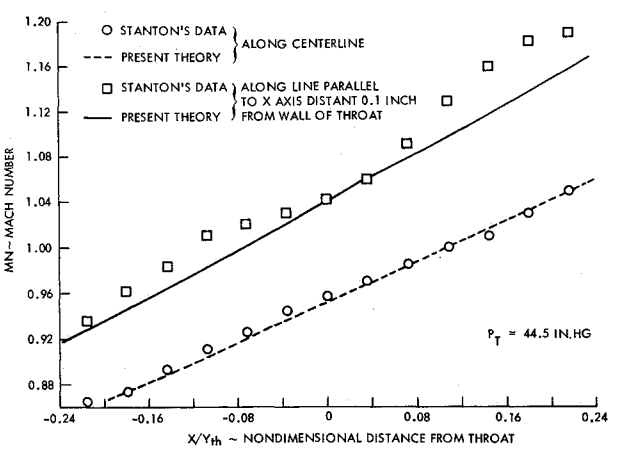

Fig. 8 Supersonic Mach number distribution in a circular-arc nozzle with $R = 4.77$.

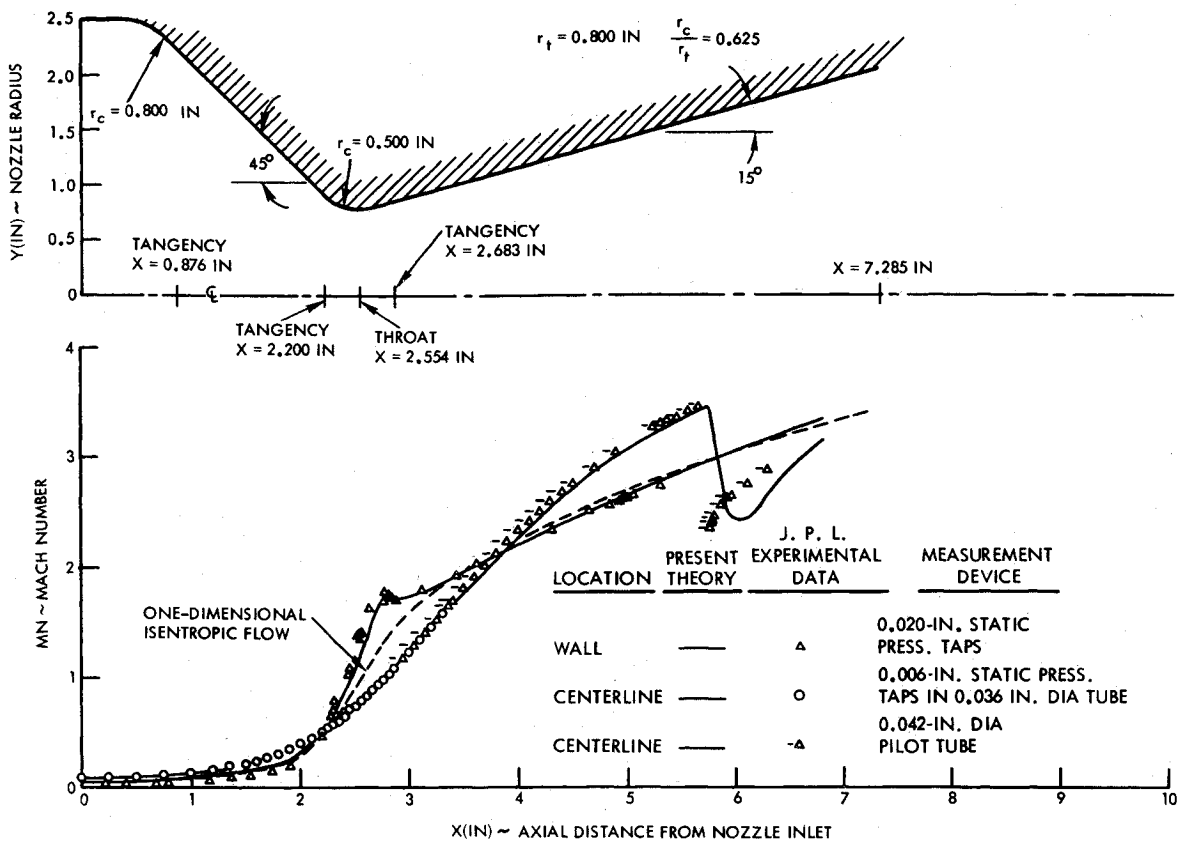

Fig. 9 Mach number distribution in a 45°–15° conical nozzle.

nozzle with R, the ratio of radius of wall curvature to throat half-height, equal to 4.77. For the case of highly subsonic flow, the significant departure between Mach number variations on longitudinal lines along the center and near the wall compares well with experiment as shown on Fig. 7.

Agreement in the supersonic case (Fig. 8) is equally good along the centerline although significant differences occur between computation and experiment for the Mach number distribution in the vicinity of the wall. A review of Stanton's paper suggests that these differences may be attributed to local flow separation which was observed during the experimentation.

Recent tests by Back et al.[6,18,19] have provided extensive Mach number distributions over a wide range of operating conditions in a 45–15 convergent-divergent conical nozzle. This nozzle, shown on Fig. 9, illustrates all the difficulties which in the past have presented numerical techniques from accurately describing the flow field throughout the entire passage. These include a rapid contraction followed by a very large throat curvature and a conical divergent section where incipient shocks form due to the coalescence of Mach lines emanating from the junction between the circular-arc throat and the divergent section.

As depicted by Fig. 9, the nozzle exhibits significant differences between the wall and centerline Mach number distributions, The flow is characterized by a rapid expansion near the wall at the throat and by a strong compression near the incipient shock at the centerline. Figure 10 displays the effect of small throat curvature ratio ($R = 0.625$) on the shape of the local constant Mach number lines. Here, the calculated subsonic Mach number profiles predict inflection points which are in good agreement with those experimentally observed by Back.[6] This excellent agreement between measured and computed Mach numbers and the accurate prediction of shock location and strength clearly demonstrate the capability of the method to handle sharply turning, inviscid, rotational flows. The resolution of the instantaneous drop in Mach number across the shock illustrated on Fig. 9 could be improved at the cost of increased computing time if the mesh size is refined beyond the value of $\Delta = 0.05$ used herein. The present solution utilized a relatively fine grid network consisting of 3000 mesh points and required a computing time of approximately 80 min.

A further application of the procedure is the accurate determination of discharge coefficients which are important in the performance predictions of propulsion nozzles. Here the present program must be coupled with a boundary-layer program to allow for both viscous losses and the flow distortion in the neighborhood of the throat. The experimental data of Back, et al.[6] yielded an average discharge coefficient of 0.985 for the 45–15 degree conical nozzle. This value represents the average for test runs conducted at the higher stagnation pressures where local

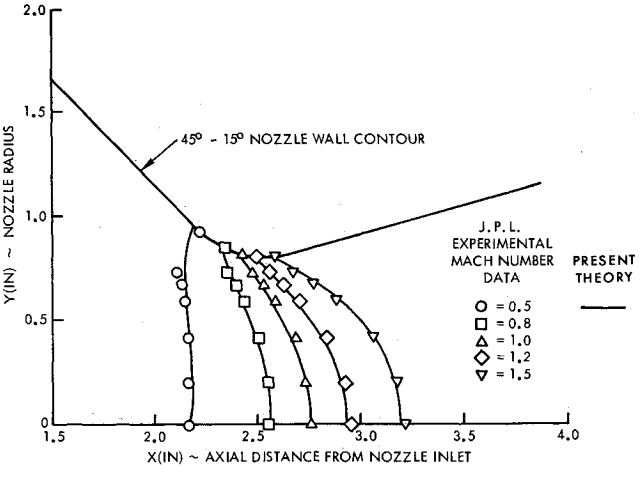

Fig. 10 Constant Mach number lines in a 45°–15° conical nozzle.

flow separation was either not encountered or found to be insignificant. The present computation yields a discharge coefficient of 0.9862 where the inviscid numerical prediction is 0.9882 and the boundary-layer correction based on Bartz's program[20] is 0.0020. The present prediction is appreciably closer to the experimental result than the previous inviscid values of 0.990 and 0.982 computed by Prozan and Kliegel, respectively, as given in Ref. 6.

Finally, Fig. 11 displays the shape and area distribution in a subsonic annular turbofan passage with large slope and reverse curvature. The corresponding inner and outer wall pressure distributions for a stagnation to exit static pressure ratio of 1.5 are predicted and compared to experimental data obtained from Ref. (1) as illustrated on Fig. 12. The good agreement shown on this figure clearly demonstrates the ability of this method to accurately solve highly subsonic inviscid flows with rapid turning.

VII. Summary and Conclusions

A time dependent method of analysis has been presented for predicting rapidly accelerating rotational flows in ducts with sharp wall curvature. Comparisons with experimental data show the method to be satisfactory for a wide variety of two-dimensional and axisymmetric duct geometries. Computing times for these solutions were significantly reduced by employing a variable mesh during the computation and ranged between a minimum of two minutes for the one-dimensional hammer shock problem (121 mesh points) to a maximum of 80 min. for the axisymmetric conical nozzle problem (3000 mesh points).

Excellent agreement is noted between the present theory and experiment for the previously unsolved case of mixed flows in nozzles involving rapid subsonic contractions, small throat curvature ratios ($R \leqq 1$) and shocks in the supersonic flow portion. Here normal comparison parameters such as axial centerline and wall Mach number distributions, sonic line position and discharge coefficient are matched to a high degree of accuracy.

On the basis of the previous analysis, the method is primarily recommended for those flow regimes where alternate procedures are unsatisfactory such as in the construction of inviscid flowfields associated with the following duct configurations: 1) sharply inclined annular ducts having reverse curvatures; 2) two-dimensional and axisymmetric passages in which arbitrarily oriented shocks may be expected to appear; and 3) rapidly converging passages connected with throat sections having small curvature ratio ($R \leqq 1$).

Finally, with the advent of larger and higher speed computers, the method appears to be promising for the solution of three-dimensional time dependent problems involving inviscid, rotational flows of mixed type.

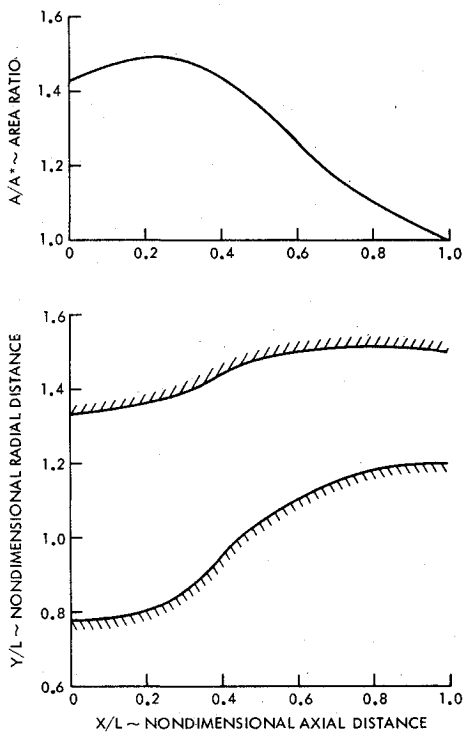

Fig. 11 Annular turbofan passage.

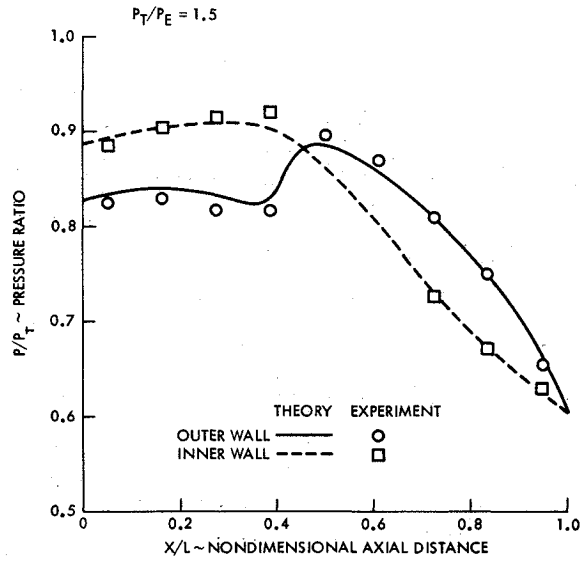

Fig. 12 Comparison between theoretical and measured passage-wall distributions in an annular curved channel.

Appendix A: Representation of the Matrices A, B, and C

As shown in Ref. 1, the evaluation of the differentials $d\bar{F}$, $d\bar{G}$ and $d\bar{H}$ in terms of the dependent variables (ρ, L, M, and E) enables the matrices $\hat{A}$, $\hat{B}$ and $\hat{C}$ to be expressed as

$$\hat{A} = \begin{bmatrix} 0 & 1 & 0 & 0 \\ \left[\frac{\tilde{g}P}{\rho} - \frac{L^2}{\rho^2} - (\gamma-1)\left(\tilde{g}\tilde{j}\frac{E}{\rho} - \frac{L^2+M^2}{\rho^2}\right)\right] & -(\gamma-3)\frac{L}{\rho} & -(\gamma-1)\frac{M}{\rho} & \tilde{g}\tilde{j}(\gamma-1) \\ -\frac{LM}{\rho^2} & \frac{M}{\rho} & \frac{L}{\rho} & 0 \\ \left[(\gamma-1)\frac{L^2+M^2}{\tilde{g}\tilde{j}\rho^2}\frac{L}{\rho} - \gamma\frac{LE}{\rho^2}\right] & \left[\frac{E+P/\tilde{j}}{\rho} - \frac{\gamma-1}{\tilde{g}\tilde{j}}\frac{L^2}{\rho^2}\right] & \frac{\gamma-1}{\tilde{g}\tilde{j}}\frac{LM}{\rho^2} & \gamma\frac{L}{\rho} \end{bmatrix} \quad \text{(A1)}$$

$$\hat{B}=\begin{bmatrix} 0 & 0 & 1 & 0 \\ -\dfrac{LM}{\rho^2} & \dfrac{M}{\rho} & \dfrac{L}{\rho} & 0 \\ \left[\dfrac{\tilde{g}P}{\rho}-\dfrac{M^2}{\rho^2}-(\gamma-1)\left(\tilde{g}\tilde{j}\dfrac{E}{\rho}-\dfrac{L^2+M^2}{\rho^2}\right)\right] & -(\gamma-1)\dfrac{L}{\rho} & -(\gamma-3)\dfrac{M}{\rho} & \tilde{g}\tilde{j}(\gamma-1) \\ \left[(\gamma-1)\dfrac{L^2+M^2}{\tilde{g}\tilde{j}\rho^2}\dfrac{M}{\rho}-\gamma\dfrac{ME}{\rho^2}\right] & -\dfrac{\gamma-1}{\tilde{g}\tilde{j}}\dfrac{LM}{\rho^2} & \left[\dfrac{E+P/\tilde{j}}{\rho}-\dfrac{\gamma-1}{\tilde{g}\tilde{j}}\dfrac{M^2}{\rho^2}\right] & \gamma\dfrac{M}{\rho} \end{bmatrix} \tag{A2}$$

and

$$\hat{C}=\begin{bmatrix} 0 & 0 & 1 & 0 \\ -\dfrac{LM}{\rho^2} & \dfrac{M}{\rho} & \dfrac{L}{\rho} & 0 \\ -\dfrac{M^2}{\rho^2} & 0 & 2\dfrac{M}{\rho} & 0 \\ \left[(\gamma-1)\dfrac{L^2+M^2}{\tilde{g}\tilde{j}\rho^2}\dfrac{M}{\rho}-\gamma\dfrac{ME}{\rho^2}\right] & -\dfrac{\gamma-1}{\tilde{g}\tilde{j}}\dfrac{LM}{\rho^2} & \left[\dfrac{E+P/\tilde{j}}{\rho}-\dfrac{\gamma-1}{\tilde{g}\tilde{j}}\dfrac{M^2}{\rho^2}\right] & \gamma\dfrac{M}{\rho} \end{bmatrix} \tag{A3}$$

where γ is the ratio of specific heats.

Appendix B: Finite-Difference Expression for W

The expression for W at time $t+\Delta t$ is obtained by using central differences to approximate the partial derivatives in Eq. (7) and is given by

$$\begin{aligned} W_{i,j}^{\tau}\Big|_{t+\Delta t} = W_{i,j}^{\tau}\Big|_{t} &- \left[b\frac{F_{i+1,j}^{\tau}-F_{i-1,j}^{\tau}}{2\Delta}+\alpha_{i,j}\frac{F_{i,j+1}^{\tau}-F_{i,j-1}^{\tau}}{2\Delta}+\beta_i\frac{G_{i,j+1}^{\tau}-G_{i,j-1}^{\tau}}{2\Delta}-\frac{\varepsilon}{y_{i,j}}H_{i,j}^{\tau}\right]\Delta t+ \\ &\left\{b\sum_{\mu=1}^{4}\frac{A_{i+1,j}^{\tau,\mu}+A_{i,j}^{\tau,\mu}}{2}\frac{1}{\Delta}\left[b\frac{F_{i+1,j}^{\mu}-F_{i,j}^{\mu}}{\Delta}+\frac{\alpha_{i+1,j}+\alpha_{i,j}}{2}\frac{1}{2}\left(\frac{F_{i+1,j+1}^{\mu}-F_{i+1,j-1}^{\mu}}{2\Delta}+\frac{F_{i,j+1}^{\mu}-F_{i,j-1}^{\mu}}{2\Delta}\right)+\frac{\beta_{i+1}+\beta_i}{2}\cdot\right.\right. \\ &\frac{1}{2}\left(\frac{G_{i+1,j+1}^{\mu}-G_{i+1,j-1}^{\mu}}{2\Delta}+\frac{G_{i,j+1}^{\mu}-G_{i,j-1}^{\mu}}{2\Delta}\right)+\frac{\varepsilon}{2}\left(\frac{H_{i+1,j}^{\mu}}{y_{i+1,j}}+\frac{H_{i,j}^{\mu}}{y_{i,j}}\right)\Bigg]-b\sum_{\mu=1}^{4}\frac{A_{i,j}^{\tau,\mu}+A_{i-1,j}^{\tau,\mu}}{2}\frac{1}{\Delta}\left[b\frac{F_{i,j}^{\mu}-F_{i-1,j}^{\mu}}{\Delta}+\frac{\alpha_{i,j}+\alpha_{i-1,j}}{2}\cdot\right. \\ &\frac{1}{2}\left(\frac{F_{i,j+1}^{\mu}-F_{i,j-1}^{\mu}}{2\Delta}+\frac{F_{i-1,j+1}^{\mu}-F_{i-1,j-1}^{\mu}}{2\Delta}\right)+\frac{\beta_i+\beta_{i-1}}{2}\frac{1}{2}\left(\frac{G_{i,j+1}^{\mu}-G_{i,j-1}^{\mu}}{2\Delta}+\frac{G_{i-1,j+1}^{\mu}-G_{i-1,j-1}^{\mu}}{2\Delta}\right)+ \\ &\left.\left.\frac{\varepsilon}{2}\left(\frac{H_{i,j}^{\mu}}{y_{i,j}}+\frac{H_{i-1,j}^{\mu}}{y_{i-1,j}}\right)\right]+\left[\alpha_{i,j}\sum_{\mu=1}^{4}\frac{A_{i,j+1}^{\tau,\mu}+A_{i,j}^{\tau,\mu}}{2}+\beta_i\sum_{\mu=1}^{4}\frac{B_{i,j+1}^{\tau,\mu}+B_{i,j}^{\tau,\mu}}{2}\right]\frac{1}{\Delta}\left[\frac{b}{2}\left(\frac{F_{i+1,j+1}^{\mu}-F_{i-1,j+1}^{\mu}}{2\Delta}+\frac{F_{i+1,j}^{\mu}-F_{i-1,j}^{\mu}}{2\Delta}\right)+\right. \\ &\frac{\alpha_{i,j+1}+\alpha_{i,j}}{2}\frac{F_{i,j+1}^{\mu}-F_{i,j}^{\mu}}{\Delta}+\beta_i\frac{G_{i,j+1}^{\mu}-G_{i,j}^{\mu}}{\Delta}+\frac{\varepsilon}{2}\left(\frac{H_{i,j+1}^{\mu}}{y_{i,j+1}}+\frac{H_{i,j}^{\mu}}{y_{i,j}}\right)\Bigg]-\left[\alpha_{i,j}\sum_{\mu=1}^{4}\frac{A_{i,j}^{\tau,\mu}+A_{i,j-1}^{\tau,\mu}}{2}+\beta_i\sum_{\mu=1}^{4}\frac{B_{i,j}^{\tau,\mu}+B_{i,j-1}^{\tau,\mu}}{2}\right] \\ &\frac{1}{\Delta}\left[\frac{b}{2}\left(\frac{F_{i+1,j}^{\mu}-F_{i-1,j}^{\mu}}{2\Delta}+\frac{F_{i+1,j-1}^{\mu}-F_{i-1,j-1}^{\mu}}{2\Delta}\right)+\frac{\alpha_{i,j}+\alpha_{i,j-1}}{2}\frac{F_{i,j}^{\mu}-F_{i,j-1}^{\mu}}{\Delta}+\beta_i\frac{G_{i,j}^{\mu}-G_{i,j-1}^{\mu}}{\Delta}+\frac{\varepsilon}{2}\left(\frac{H_{i,j}^{\mu}}{y_{i,j}}+\frac{H_{i,j-1}^{\mu}}{y_{i,j-1}}\right)\right]+ \\ &\left.\left.\frac{\varepsilon}{y_{i,j}}\sum_{\mu=1}^{4}C_{i,j}^{\tau,\mu}\left[b\frac{F_{i+1,j}^{\mu}-F_{i-1,j}^{\mu}}{2\Delta}+\alpha_{i,j}\frac{F_{i,j+1}^{\mu}-F_{i,j-1}^{\mu}}{2\Delta}+\beta_i\frac{G_{i,j+1}^{\mu}-G_{i,j-1}^{\mu}}{2\Delta}+\frac{H_{i,j}^{\mu}}{y_{i,j}}\right]\right\}\frac{\Delta t^2}{2} \end{aligned} \tag{B1}$$

References

[1] Serra, R. A., "The Determination of Internal Gas Flows by a Transient Numerical Technique," Ph.D. thesis, June 1970, Rensselaer Polytechnic Inst., Troy, N.Y.

[2] Lax, P. D. and Wendroff, B., "Difference Schemes with High Order of Accuracy for Solving Hyperbolic Equations," CIMS Report NY0-9759, July 1962, New York Univ., New York.

[3] Burstein, S. Z., "Finite-Difference Calculations for Hydrodynamic Flows Containing Discontinuities," *Journal of Computational Physics*, Vol. 1, No. 2, Nov. 1966, pp. 198–222.

[4] Moretti, G., Migdal, D., and Klein, K., "Time-Dependent Calculations for Transonic Nozzle Flow," *AIAA Journal*, Vol. 7, No. 2, Feb. 1969, pp. 372–374.

[5] Stephens, J. T., "Analytical Results for Transonic Flow Fields in Rocket Motors," TM LMSC/HREC A784847, 1967, Lockheed Missle & Space Co., Huntsville, Ala.

[6] Cuffel, R. F., Back, L. H., and Massier, P. F., "Transonic Flow Field in a Supersonic Nozzle with Small Throat Radius of Curvature," *AIAA Journal*, Vol. 7, No. 7, July 1969, pp. 1364–1366.

[7] Wehofer, S. and Moger, W. C., "Transonic Flow in Conical Convergent and Convergent-Divergent Nozzles with Nonuniform Inlet Conditions," AIAA Paper 70-635, San Diego, Calif., 1970.

[8] Burstein, S. Z., "Numerical Calculations of Multidimensional Shocked Flow," *AIAA Journal*, Vol. 12, No. 12, Dec. 1964, pp. 2111–2117.

[9] Edelman, R. B., Abbett, M. J., Weilerstein, G., Fortune, O., and Genovese, J., "Some Aspects of Viscous Chemically Reacting Moderate Altitude Rocket Exhaust Plumes," March 1970, General Applied Science Labs., Westbury, N.Y.

[10] Friedrichs, K. O., "Symmetric Positive Linear Differential Equations," *Comm. Pure and Applied Mathematics*, Vol. XI, 1958, pp. 333–418.

[11] Courant, R. and Hilbert, D., "Hyperbolic Differential Equations in More Than Two Independent Variables," *Methods of Mathematical Physics*, Vol. II, Interscience, New York, 1962, pp. 675.

[12] Ganz, A. and Serra, R. A., "A Class of Admissible Boundary Conditions to the Transient Initial Value Problem," unpublished Memo, June 1971, Pratt and Whitney Aircraft, East Hartford, Conn.
[13] Rudinger, G., "Interruption of a Supersonic Flow," *Wave Diagrams for Nonsteady Flow in Ducts*, Van Nostrand, New York, 1955, pp. 208–213.
[14] Cherry, T. M., "Some Nozzle Flows Found by the Hodograph Method," *Journal of the Australian Mathematical Society*, Vol. 1, Pt. 1, 1959, pp. 80–94.
[15] Thompson, P. A., "Transonic Flow in Curved Channels," Paper 67 FE-11, Chicago, Ill., 1967, ASME.
[16] Jacobs, W., "Geschwindigkeitsverteilungen in zweidimensionalen Gekrümmten Lavaldüsen," *Jahrbuck wiss. Gesellschaft Luftfahrt*, 1954, pp. 57–62.
[17] Stanton, T. E., "The Variation of Velocity in the Neighborhood of the Throat of a Constriction in a Wind Channel," R and M 1388, May 1930, Aeronautical Research Council.
[18] Back, L. H., Massier, P. F., and Gier, H. L., "Comparison of Measured and Predicted Flows Through Conical Supersonic Nozzles, with Emphasis on the Transonic Region," *AIAA Journal*, Vol. 3, No. 9, Sept. 1965, pp. 1606–1614.
[19] Back, L. H. and Cuffel, R. F., "Detection of Oblique Shocks in a Conical Nozzle with a Circular-Arc Throat," *AIAA Journal*, Vol. 4, No. 12, Dec. 1966, pp. 2219–2221.
[20] Bartz, D. R., "An Approximate Solution of Compressible Turbulent Boundary-Layer Development and Convective Heat Transfer in Convergent-Divergent Nozzles," *Transactions of the ASME*, 1955, pp. 1235–1245.

MAY 1972 AIAA JOURNAL VOL. 10, NO. 5

Jet-Flapped Wings in Very Close Proximity to the Ground

TERUHIKO KIDA* AND YOSHIHIRO MIYAI†
University of Osaka Prefecture, Osaka, Japan

The method of matched asymptotic expansions is applied to the problem of jet-flapped wings of finite span in very close proximity to the ground. For the linearization of this problem, the order of small parameters, the angle of attack and jet deflection, are assumed to be smaller than the ratio of the ground clearance to the root chord. This linearized problem is solved as a direct problem represented by a source distribution on the upper surface of the wing and jet sheet with concentrated sources around the leading and side edges plus a separate confined channel flow region under the wing and jet sheet. The two-dimensional, jet-flapped airfoil is examined in detail, and the calculated lift coefficients lie within 5% of corresponding results by Lissaman.[1] In the three-dimensional case, a simple analytic solution is obtained for a flat plate semi-elliptic wing with a straight trailing edge, zero angle of attack and uniform momentum distribution of the jet. Spanwise lift distributions and lift coefficients are derived and the distributions of the jet momentum are discussed for minimum induced drag.

Introduction

RECENTLY, the possibility of using aerodynamics to support a high-speed ground transportation vehicle gives rise to an interesting class of problems in which a lifting surface translates in close proximity to a solid boundary.[2,3] The problem of airfoil section in ground proximity without jet flap (ram airfoils) has already been the object of several studies. In Ref. 4, the potential flow problem for two-dimensional flat plates in ground proximity is solved exactly by conformal transformations. Recently, three-dimensional problems have been solved by lifting surface theory with solutions generally requiring a high-speed computer.[5]

A jet flap is formed by a high-speed jet which emerges from a wing through a thin slit along its trailing edge. It affects the lift both by direct momentum reaction on the internal ducting and by changing the pressure distribution on the outer surface of the wing (i.e., supercirculation). Since this can increase the lift while most of the jet thrust is recovered as propulsion, the jet flap represents a way of combining the lifting and propulsive systems of jet aircraft. Early theoretical work for a two-dimensional wing in ground proximity with jet flap was done by Huggett[6] and others using the principle of a simple lifting line. Since then, Lissaman and the present authors gave an extension (by conformal transformation) to this ground effect problem,[1,7] and we applied the principle of the equivalence between the jet flap and the mechanical flap to this problem.[8]

All of these approaches are quite reasonable for wings which are not too close to the ground, such as might be encountered with an airfoil during takeoff and landing. However, when a lifting surface is designed to take advantage of ground effect the greatest interest lies in very close proximity. The theoretical work without jet flap for this case was done by Widnall and Barrows,[2,3] and the two-dimensional wing both with and without jet flap was studied by Cooke[9] using the principle of small perturbation technique. In the latter work, the basic physical limitation occurs when the jet curtain impinges on the ground and the numerical calculations for the jet-flapped airfoil have only been made for the half ground clearance to the chord, for the numerical methods are more complicated as the ground is approached.

The expected range of operation of high-speed ground transportation vehicles is such that the ratio of the ground clearance of the root chord is less than 0.1.[2,10] Also, while theoretical analysis of three-dimensional, jet-flapped wings have been developed by Maskell and Spence,[11] the effect of ground proximity has not been considered. In the present paper, the linearized ground effect problem of two- and three-dimensional wings is solved, using the method of matched asymptotic expansions as applied by Widnall and Barrows[2,3] to ram wings without jet flap. An important feature of the present method is that this problem is a direct problem, involving a known source distribution on the upper surface of the wing and jet sheet with concentrated sources around the leading and side edges plus a separate confined channel flow region under the wing and jet sheet. Thus, even for a general airfoil, the difficulties of inverting an integral equation are avoided. Clearly, special expansions are required in the flow region near the trailing edge which are different from those of Ref. 2, because the Kutta Joukowski hypothesis at the trailing edge is not imposed for the jet-flapped wing and the boundary condition that the jet emerges from this edge at a deflection angle is imposed at this point.

Received June 1, 1971; revision received December 18, 1971.
Index category: Ground Effect Machines.
* Lecturer of Mechanical Engineering.
† Professor of Mechanical Engineering.